arXiv:2111.00278v3 [cs.AI] 20 Feb 2022

A Decentralized Reinforcement Learning Framework for Efficient Passage of Emergency Vehicles

Haoran Su[†*], **Yaofeng Desmond Zhong**[§], **Biswadip Dey**[§], **Amit Chakraborty**[§]
[†] New York University | [§] Siemens Corporation, Technology
haoran.su@nyu.edu, (yaofeng.zhong, biswadip.dey, amit.chakraborty)@siemens.com

Abstract

Emergency vehicles (EMVs) play a critical role in a city's response to time-critical events such as medical emergencies and fire outbreaks. The existing approaches to reduce EMV travel time employ route optimization and traffic signal pre-emption without accounting for the coupling between route these two subproblems. As a result, the planned route often becomes suboptimal. In addition, these approaches also do not focus on minimizing disruption to the overall traffic flow. To address these issues, we introduce *EMVLight* in this paper. This is a decentralized reinforcement learning (RL) framework for simultaneous dynamic routing and traffic signal control. EMVLight extends Dijkstra's algorithm to efficiently update the optimal route for an EMV in real-time as it travels through the traffic network. Consequently, the decentralized RL agents learn network-level cooperative traffic signal phase strategies that reduce EMV travel time and the average travel time of non-EMVs in the network. We have carried out comprehensive experiments with synthetic and real-world maps to demonstrate this benefit. Our results show that EMVLight outperforms benchmark transportation engineering techniques as well as existing RL-based traffic signal control methods.

1 Introduction

As any reduction in the travel time of an EMV increases the likelihood that it would save someone's life or reduce property loss, there is a significant benefit in reducing the average EMV travel time on increasingly crowded roads. To tackle this challenge, existing approaches rely upon – *route optimization* which uses graph-theoretic tools to find the fastest path; and *traffic signal pre-emption* which alters the traffic signals to prioritize EMV passage and improves overall safety at the intersections. Please see Section S1 for additional details about the existing approaches on route optimization and traffic signal control. However, the constantly changing traffic conditions can significantly affect the optimality of a route prescribed by route optimization. In addition, traffic signal pre-emption also changes the optimal route by causing serious disruptions to the traffic flow.

To address these issues and achieve efficient EMV passage, we introduce **EMVLight** which is a decentralized multi-agent RL framework with a dynamic routing algorithm to control traffic signal phases. We introduce a computationally efficient dynamic routing algorithm and an RL-based traffic signal pre-emption strategy to not only reduce *EMV travel time* but also to reduce the *average travel time of non-EMVs*. Our experiments demonstrate that EMVLight outperforms traditional traffic engineering methods and existing RL methods on both metrics under different traffic configurations.

[*]This study is conducted with his internship with Siemens. He is also sponsored by DDETFP by U.S. Department of Transportation Federal Highway Administration.

Artificial Intelligence for Humanitarian Assistance and Disaster Response Workshop, NeurIPS 2021.

2 Application Context

Emergency response time is the key indicator of a city's emergency management capability. Reducing response time saves lives and prevents property loss. For instance, the survivor rate from a sudden cardiac arrest without treatment drops 7% - 10% for every minute elapsed, and there is barely any chance to survive after 8 minutes [1]. The time interval for an *emergency vehicle (EMV)*, e.g., ambulances, fire trucks, and police cars, to travel from a rescue station to an incidence site, i.e., the *EMV travel time*, accounts for a significant portion of the emergency response time. However, overpopulation and urbanization have been exacerbating road congestion, making it more and more challenging to reduce the average EMV travel time [2]. There is a severe urgency and significant benefit in reducing the average EMV travel time on increasingly crowded roads.

3 Preliminaries

Traffic map, Link, Lane: A traffic map can be represented by a graph $G(\mathcal{V}, \mathcal{E})$, with intersections as nodes and road segments between intersections as edges. We refer to a one-directional road segment between two intersections as a link. A link has a fixed number of lanes, denoted as $h(l)$ for lane l. Fig. 1 shows 8 links and each link has 2 lanes.

Traffic Movements: A traffic movement (l, m) is defined as the traffic traveling across an intersection from an incoming lane l to an outgoing lane m. The intersection shown in Fig. 1 has 24 permissible traffic movements. The set of all permissible traffic movements of an intersection is denoted as $\mathcal{M}$.

Traffic Signal Phase: A traffic signal phase is defined as the set of permissible traffic movements. As shown in Fig. 2, an intersection with 4 links has 8 phases.

Pressure of an incoming lane: The pressure of an incoming lane l measures the unevenness of vehicle density between lane l and corresponding outgoing lanes in permissible traffic movements. The vehicle density of a lane is $x(l)/x_{max}(l)$, where $x(l)$ is the number of vehicles on lane l and $x_{max}(l)$ is the vehicle capacity on lane l, which is related to the length of a lane. Then the pressure of an incoming lane l is

$$w(l) = \left| \frac{x(l)}{x_{max}(l)} - \sum_{\{m|(l,m)\in\mathcal{M}\}} \frac{1}{h(m)} \frac{x(m)}{x_{max}(m)} \right|,$$

where $h(m)$ is the number of lanes of the outgoing link which contains m. This concept has been explained in Fig. 1 wherein $h(m) = 2$ for all the outgoing lanes.

Pressure of an intersection: The pressure of an intersection (P) is the average of the pressure of all incoming lanes. It indicates the unevenness of vehicle density between incoming and outgoing lanes in an intersection. Intuitively, reducing the pressure leads to more evenly distributed traffic, which indirectly reduce congestion and average travel time of vehicles.

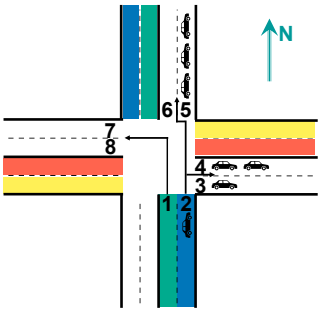


Figure 1: This figure illustrates traffic movements through an intersection and an example pressure calculation for incoming lane #2. Vehicles on Lane 1 are turning left, and vehicles on Lane 2 may either go straight or turn right. After turning right, vehicles can enter either lane. Thus, the incoming link from South has the following traffic movement: (1, 7), (1, 8), (2, 5), (2, 6), (2, 3), (2, 4). Assuming each lane has the maximum capacity of 5, the lane pressure for Lane 2 can then be calculated as: $w(2) = |1/5 - (1/2) * (1/5 + 2/5) - (1/2) * (3/5 + 0/5)| = 0.4$.

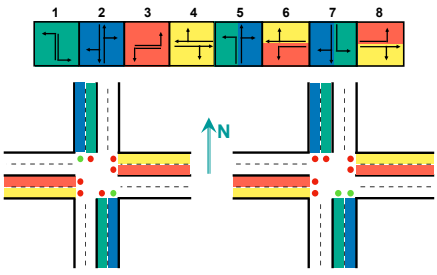


Figure 2: *Top* panel of this figure shows the 8 signal phases for a 4-way intersection. The *bottom-left* and *bottom-right* panels show phase 2 and 5, respectively.

4 Dynamic Routing

A traffic network can be perceived as a weighted graph with the weights representing the *intra-link travel time*, i.e., the EMV travel time along each link which has been estimated from the number of vehicles on that link. This enables the use of Dijkstra's algorithm for finding solutions to the EMV routing problem. However, continuously changing traffic conditions keep changing the intra-link

travel time and thereby render the weighted graph dynamic. Although this challenge can be addressed by running Dijkstra's algorithm repeatedly as the EMV travels through the network, it is not viable from a computational perspective. In this work, we extend Dijkstra's algorithm to efficiently update the optimal route based on the most recent information about the intra-link travel times (Algorithm 1). We first run Dijkstra's algorithm to obtain the *estimated time of arrival (ETA)* from each intersection to the destination and the *next intersection* along the shortest path. Since a sequence of processes, including call-taker processing, are performed before an EMVs is dispatched, it is reasonable to assume that this process can be done before an EMV starts to travel. Once an EMV has started its journey, we update ETA and Next values for each intersection. As these updates only depend on information about neighboring intersections, they are computationally inexpensive and can be executed in parallel. Please see Section S5 for further details about how intra-link travel time is estimated in real time.

Algorithm 1: Dynamic Dijkstra's for EMV routing

Input :

$G = (\mathcal{V}, \mathcal{E})$	traffic map as a graph
$T^t = [T^t_{ij}]$	intra-link travel time at time t
i_d	index of the destination

Output :

$\mathsf{ETA}^t = [\mathsf{ETA}^t_i]$	ETA of each intersection
$\mathsf{Next}^t = [\mathsf{Next}^t_i]$	next intersection to go from each intersection

`/* pre-population */`

$\mathsf{ETA}^0, \mathsf{Next}^0 = \texttt{Dijkstra}(G, T^0, i_d)$

`/* dynamic routing */`

for $t = 0 \to T$ **do**

  foreach $i \in \mathcal{V}$ **do (in parallel)**

    $\mathsf{ETA}^{t+1}_i \leftarrow \min_{(i,j)\in\mathcal{E}}(\mathsf{ETA}^t_j + T^t_{ji})$

    $\mathsf{Next}^{t+1}_i \leftarrow \arg\min_{\{j|(i,j)\in\mathcal{E}\}}(\mathsf{ETA}^t_j + T^t_{ji})$

5 Setting up the RL Problem

While dynamic routing directs the EMV to the destination, it does not take into account the possible wait times due to red lights at the intersections. Thus, traffic signal pre-emption is also required for the EMV to arrive at the destination in the least amount of time. However, since traditional pre-emption only focuses on reducing the EMV travel time, it can significantly increase the average travel time of non-EMVs. In this work, we set up traffic signal control for efficient EMV passage as a decentralized RL problem. In our formulation, we employ multiple RL agents (one for each intersection) that work cooperatively to reduce both EMV travel time and the average travel time of non-EMVs.

5.1 Types of agents for EMV passage

Whenever an EMV is travelling through the traffic network, the agents that control the traffic signal at the intersections are grouped into 3 distinct categories based on EMV location and routing (Fig. 3). An agent is categorized as a *primary pre-emption agent* i_p if an EMV is travelling on one of its incoming links. The agent at the next intersection along the optimal route is categorized as a *secondary pre-emption agent*, i.e. $i_s = \mathsf{Next}_{i_p}$. The rest of the agents are *normal agents*. Each of these agent types has different local goals which is captured into their reward functions.

5.2 Agent design

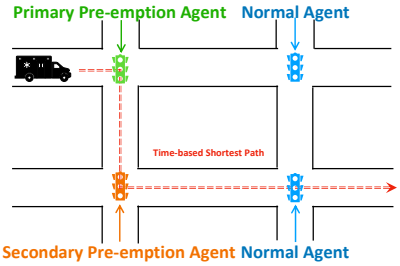


Figure 3: EMVLight employs 3 types of agents.

• **State:** The state of an agent i at time t includes the number of vehicles on each of the incoming and outgoing lanes at intersection i, the distance of the EMV to the intersection, the estimated time of arrival (ETA), and which link the EMV will be routed to (Next). Therefore, we have

$$s^t_i = \{x^t(l), x^t(m), d^t_{\text{EMV}}[L_{ji}], \mathsf{ETA}^{t'}_i, \mathsf{Next}^{t'}_i\},$$

where L_{ji} denotes the links incoming to intersection i, and with a slight abuse of notation l and m denote the set of incoming and outgoing lanes, respectively. For primary pre-emption agents, one of the elements of d^t_{EMV} represents the distance of the EMV to the intersection in the corresponding link and the rest of the elements are set to -1. For secondary pre-emption agents and normal agents, every element of d^t_{EMV} is set to -1.

• **Action:** We define the action of an agent as one of the 8 signal phases shown in Fig. 2. This enables more flexible signal patterns as compared to the traditional cyclical patterns. Also, due to safety concerns, once a signal phase has been initiated, it remains unchanged for certain minimum amount

of time.

• **Reward:** PressLight has shown that minimizing the pressure can encourage efficient vehicle passage [3]; here we adopt a similar approach for the normal agents. For secondary pre-emption agents, we additionally encourage less vehicle on the link where the EMV is about to enter in order to encourage efficient EMV passage. For primary pre-emption agents, we assign a unit penalty at each time step to encourage fast EMV passage. Thus, the local reward for agent i at time t is defined as

$$r_i^t = \begin{cases} -P_i^t & i \notin \{i_p, i_s\}, \text{ i.e., Normal Agent,} \\ -\beta P_i^t - \frac{1-\beta}{|L_{i_p i}|} \sum_{l \in L_{i_p i}} \frac{x(l)}{x_{max}(l)} & i = i_s, \text{ i.e., Secondary pre-emption agent,} \\ -1 & i = i_p, \text{ i.e., Primary pre-emption agent.} \end{cases} \quad (1)$$

5.3 Multi-agent Advantage Actor-critic

To realize the decentalized RL framework, we adopt a multi-agent advantage actor-critic (MA2C) approach that is similar to [4]. In this formulation, the RL agent at intersection i learns a policy π_{θ_i} (actor) and the corresponding value function V_{ϕ_i} (critic), where θ_i and ϕ_i are learnable neural network parameters. In our formulation, the local state includes dynamic routing information and the local reward encourages efficient passage of the EMV, whereas [4] focuses on a general traffic signal control problem with no EMV considered. Please see Section S3 for additional details.

6 Experiments and Results

To evaluate performance of our proposed EMVLight framework, we carry out experiments using the *SUMO* [5] simulation tool that can simulate traffic dynamics in both microscopic and macroscopic settings. In our experiments, the decentralized RL agents collect observations from SUMO and the preferred signal phases are then fed back into the traffic simulator.

6.1 Datasets and Maps Descriptions

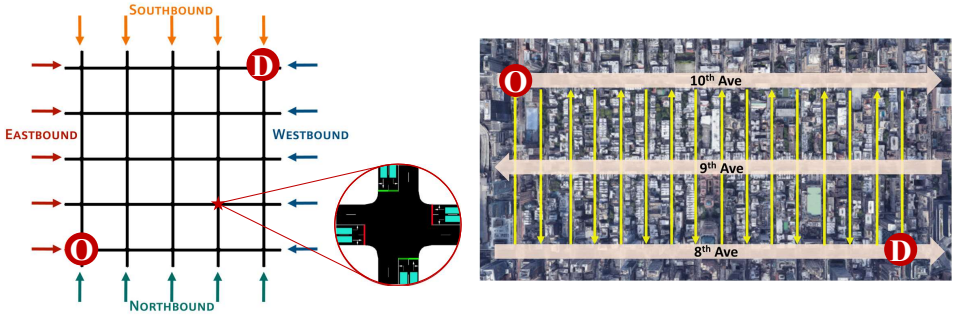
We carry out our experiments using both synthetic and real-world maps.

Synthetic Grid: We first consider a synthetic grid of size 5×5, where the intersections are connected with bi-directional links with each link containing two lanes (Fig. 4a). For the synthetic map, we consider two different traffic flow configurations with peak/non-peak flow values of 240/200 *veh/lane/hr* and 320/120 *veh/lane/hr*. In both configurations, vehicles enter the grid via north/south-bound links and leave the grid via east/west-bound links. The traffic for this map has a time span of 1200s and the EMV is dispatched at $t = 600s$ to ensure roads are compacted before the EMV starts travelling; also, the peak flow occurs between 400s-800s.

Manhattan Map: This is a 16×3 traffic network extracted from Manhattan Hell's Kitchen area (Fig. 4b). In this traffic network, intersections are connected by 16 one-way 2-lane streets and 3 one-way 4-lane avenues. The traffic flow for this map is generated from open-source NYC taxi data (*https://traffic-signal-control.github.io/*).

6.2 Baselines

As RL-based approaches for efficient EMV passage do not yet exist, we select traditional methods and RL methods for individual subproblems and combine them to set up baselines. For traffic signal



(*a*) (*b*)

Figure 4: *Left*: the synthetic grid$_{5\times5}$. *Right*: an intersection illustration in SUMO, the teal area are inductive loop detected area. Origin and destination for EMV are labeled. Manhattan map: a 16-by-3 traffic network in Hell's Kitchen area. Origin and destination for the EMV dispatching are labeled as "**O**" and "**D**", respectively.

pre-emption, we use *Walabi* [6], a rule-based method that implements *Green Wave* [7] for EMVs. We then integrate Walabi (*W*) with combinations of *routing* and *traffic signal control* strategies. For routing, we consider 2 baselines – a *Static* routing based on A*; and a *dynamic* routing by running A* every $50s$. For controlling the traffic signals, we consider the following 4 baseline approaches – a cyclical *fixed time (FT)* traffic phases with random offset that splits all phases with an predefined green ratio [8]; a network-level signal control strategy based on *max pressure (MP)* that smoothens congestion by aggressively selecting the phase with the maximum pressure [9]; a Q-learning based *coordinated learner (CL)* that directly learns joint local value functions for adjacent intersections [10]; and finally *PressLight (PL)* which uses RL to optimize the pressure at each intersection [3].

6.3 Results

We evaluate performance of models under two metrics: *EMV travel time*, which reflects routing and pre-emption ability, and *average travel time*, which indicates the ability of traffic signal control for efficient vehicle passage. The performance of our EMVLight and the baselines in both the synthetic and the Manhattan map is shown in Table 1. The results of all methods are averaged over five independent runs and RL methods are tested with random seeds. We observe that EMVLight outperforms all baseline models under both metrics.

Method	EMV Travel Time [s]			Average Travel Time [s]		
	Config 1	Config 2	Mahanttan	Config 1	Config 2	Mahanttan
No EMV + FT	N/A	N/A	N/A	353.43	371.13	1649.64
W + Static + FT	257.20	272.00	487.20	372.19	389.13	1711.03
W + Static + MP	255.00	269.00	461.80	349.38	352.54	708.13
W + Static + GRL	281.20	286.20	492.20	503.35	524.26	2013.54
W + Static + PL	276.00	282.20	476.00	358.18	369.45	1410.76
W + Dynamic + FT	229.60	231.20	442.60	370.09	293.40	1699.30
W + Dynamic + MP	226.20	234.60	438.80	345.45	348.43	721.32
W + Dynamic + GRL	273.40	269.60	450.20	514.29	536.78	1987.86
W + Dynamic + PL	251.20	257.80	436.20	359.31	342.59	1412.12
EMVLight	**198.60**	**192.20**	**391.80**	**322.40**	**318.76**	**681.23**

Table 1: *Performance comparison of different methods evaluated on four configurations in the synthetic traffic grid as well as Manhattan Map. For both metrics, the lower value indicates better performance. The lowest values are highlighted in bold. The average travel time of Manhattan map (1649.64) is retrieved from data.*

In terms of EMV travel time T_{EMV}, the dynamic routing baseline performs better than static routing baselines. This is expected since dynamic routing considers the time-dependent nature of traffic conditions and update optimal route accordingly. EMVLight further reduces EMV travel time by 18% in average as compared to dynamic routing baselines. This advantage in performance can be attributed to the design of secondary pre-emption agents. This type of agents learn to "reserve a link" by choosing signal phases that help clear the vehicles in the link to encourage high speed EMV passage (Eqn. (1)).

As for average travel time T_{avg}, we first notice that the traditional pre-emption technique (W+Static+FT) indeed increases the average travel time by around 10% as compared to a traditional Fix Time strategy without EMV (denoted as "FT w/o EMV" in Table 1), thus decreasing the efficiency of vehicle passage. Different traffic signal control strategies have a direct impact on overall efficiency. Fixed Time is designed to handle steady traffic flow. Max Pressure, as a SOTA traditional method, outperforms Fix Time and, surprisingly, outperforms both RL baselines in terms of overall efficiency. This shows that pressure is an effective indicator for reducing congestion and this is why we incorporate pressure in our reward design. Coordinate Learner performs the worst probably because its reward is not based on pressure. PressLight doesn't beat Max Pressure because it has a reward design that focuses on smoothing vehicle densities along a major direction, e.g. an arterial. Grid networks with the presence of EMV make PressLight less effective. Our EMVLight improves its pressure-based reward design to encourage smoothing vehicle densities of all directions for each intersection. This enable us to achieve an advantage of 5% over our best baselines (Max Pressure).

7 Conclusion

In this paper, we proposed a decentralized reinforcement learning framework, EMVLight, to facilitate the efficient passage of EMVs and reduce traffic congestion at the same time. Leveraging the multi-agent A2C framework, agents incorporate dynamic routing and cooperatively control traffic signals

to reduce EMV travel time and average travel time of non-EMVs. Evaluated on both synthetic and real-world map, EMVLight significantly outperforms the existing methods. Future work will explore more realistic microscopic interaction between EMV and non-EMVs, efficient passage of multiple EMVs and closing the sim-to-real gap.

References

[1] G. Nichol, E. Thomas, C. W. Callaway, J. Hedges, J. L. Powell, T. P. Aufderheide, T. Rea, R. Lowe, T. Brown, J. Dreyer *et al.*, "Regional variation in out-of-hospital cardiac arrest incidence and outcome," *Jama*, vol. 300, no. 12, pp. 1423–1431, 2008.

[2] N. Analytics, "End-to-end response times," https://www1.nyc.gov/site/fdny/about/resources/data-and-analytics/end-to-end-response-times.page, 2021.

[3] H. Wei, C. Chen, G. Zheng, K. Wu, V. Gayah, K. Xu, and Z. Li, "Presslight: Learning max pressure control to coordinate traffic signals in arterial network," in *Proceedings of the 25th ACM SIGKDD International Conference on Knowledge Discovery & Data Mining*, 2019, pp. 1290–1298.

[4] T. Chu, J. Wang, L. Codecà, and Z. Li, "Multi-agent deep reinforcement learning for large-scale traffic signal control," *IEEE Transactions on Intelligent Transportation Systems*, 2019.

[5] P. A. Lopez, M. Behrisch, L. Bieker-Walz, J. Erdmann, Y.-P. Flötteröd, R. Hilbrich, L. Lücken, J. Rummel, P. Wagner, and E. Wießner, "Microscopic traffic simulation using sumo," in *2018 21st International Conference on Intelligent Transportation Systems (ITSC)*. IEEE, 2018, pp. 2575–2582.

[6] L. Bieker-Walz and M. Behrisch, "Modelling green waves for emergency vehicles using connected traffic data," *EPiC Series in Computing*, vol. 62, pp. 1–11, 2019.

[7] F. Corman, A. D'Ariano, D. Pacciarelli, and M. Pranzo, "Evaluation of green wave policy in real-time railway traffic management," *Transportation Research Part C: Emerging Technologies*, vol. 17, no. 6, pp. 607–616, 2009.

[8] R. P. Roess, E. S. Prassas, and W. R. McShane, *Traffic engineering*. Pearson/Prentice Hall, 2004.

[9] P. Varaiya, "Max pressure control of a network of signalized intersections," *Transportation Research Part C: Emerging Technologies*, vol. 36, pp. 177–195, 2013.

[10] E. Van der Pol and F. A. Oliehoek, "Coordinated deep reinforcement learners for traffic light control," *Proceedings of Learning, Inference and Control of Multi-Agent Systems (at NIPS 2016)*, 2016.

[11] J. Wang, W. Ma, and X. Yang, "Development of degree-of-priority based control strategy for emergency vehicle preemption operation," *Discrete dynamics in nature and society*, vol. 2013, 2013.

[12] H. Mu, Y. Song, and L. Liu, "Route-based signal preemption control of emergency vehicle," *Journal of Control Science and Engineering*, vol. 2018, pp. 1–11, 04 2018.

[13] E. Kwon, S. Kim, and R. Betts, "Route-based dynamic preemption of traffic signals for emergency vehicle operations," in *Transportation Research Board 82nd Annual MeetingTransportation Research Board*, 2003.

[14] A. Jotshi, Q. Gong, and R. Batta, "Dispatching and routing of emergency vehicles in disaster mitigation using data fusion," *Socio-Economic Planning Sciences*, vol. 43, no. 1, pp. 1 – 24, 2009.

[15] N. A. M. Nordin, Z. A. Zaharudin, M. A. Maasar, and N. A. Nordin, "Finding shortest path of the ambulance routing: Interface of a-star algorithm using c programming," in *2012 IEEE Symposium on Humanities, Science and Engineering Research*. IEEE, 2012, pp. 1569–1573.

[16] A. K. Ziliaskopoulos and H. S. Mahmassani, "Time-dependent, shortest-path algorithm for real-time intelligent vehicle highway system applications," in *Transportation Research Record*, 1993, pp. 94–100.

[17] G. Musolino, A. Polimeni, C. Rindone, and A. Vitetta, "Travel time forecasting and dynamic routes design for emergency vehicles," *Procedia-Social and Behavioral Sciences*, vol. 87, pp. 193–202, 2013.

[18] A. Haghani, H. Hu, and Q. Tian, "An optimization model for real-time emergency vehicle dispatching and routing," in *82nd annual meeting of the Transportation Research Board, Washington, DC*. Citeseer, 2003.

[19] S. Koh, B. Zhou, H. Fang, P. Yang, Z. Yang, Q. Yang, L. Guan, and Z. Ji, "Real-time deep reinforcement learning based vehicle navigation," *Applied Soft Computing*, vol. 96, p. 106694, 2020.

[20] M. Asaduzzaman and K. Vidyasankar, "A priority algorithm to control the traffic signal for emergency vehicles," in *2017 IEEE 86th Vehicular Technology Conference (VTC-Fall)*, 2017, pp. 1–7.

[21] L. Lu and S. Wang, "Literature review of analytical models on emergency vehicle service: Location, dispatching, routing and preemption control," in *2019 IEEE Intelligent Transportation Systems Conference (ITSC)*, 2019, pp. 3031–3036.

[22] S. Humagain, R. Sinha, E. Lai, and P. Ranjitkar, "A systematic review of route optimisation and pre-emption methods for emergency vehicles," *Transport reviews*, vol. 40, no. 1, pp. 35–53, 2020.

[23] C. You, Q. Yang, L. Gjesteby, G. Li, S. Ju, Z. Zhang, Z. Zhao, Y. Zhang, W. Cong, G. Wang *et al.*, "Structurally-sensitive multi-scale deep neural network for low-dose CT denoising," *IEEE Access*, 2018.

[24] L. Cheng and C. You, "Hybrid non-linear dimensionality reduction method framework based on random projections," in *2016 IEEE International Conference on Cloud Computing and Big Data Analysis (ICCCBDA)*. IEEE, 2016, pp. 43–48.

[25] G. Li, S. Luo, C. You, M. Getzin, L. Zheng, G. Wang, and N. Gu, "A novel calibration method incorporating nonlinear optimization and ball-bearing markers for cone-beam ct with a parameterized trajectory," *Medical physics*, 2019.

[26] L. Cheng, C. You, and Y. Guan, "Random projections for non-linear dimensionality reduction," *International Journal of Machine Learning and Computing*, vol. 6, no. 4, pp. 220–225, 2016.

[27] L. Cheng, C. You, Y. Guan, and Y. Yu, "Body activity recognition using wearable sensors," in *2017 Computing Conference*. IEEE, 2017, pp. 756–765.

[28] C. You, L. Yang, Y. Zhang, and G. Wang, "Low-Dose CT via Deep CNN with Skip Connection and Network in Network," in *Developments in X-Ray Tomography XII*. International Society for Optics and Photonics, 2019.

[29] C. You, G. Li, Y. Zhang, X. Zhang, H. Shan, M. Li, S. Ju, Z. Zhao, Z. Zhang, W. Cong *et al.*, "CT super-resolution GAN constrained by the identical, residual, and cycle learning ensemble (gan-circle)," *IEEE Transactions on Medical Imaging*, 2019.

[30] Q. Lyu, C. You, H. Shan, Y. Zhang, and G. Wang, "Super-resolution mri and ct through gan-circle," in *Developments in X-ray tomography XII*. International Society for Optics and Photonics, 2019.

[31] C. You, J. Yang, J. Chapiro, and J. S. Duncan, "Unsupervised wasserstein distance guided domain adaptation for 3d multi-domain liver segmentation," in *Interpretable and Annotation-Efficient Learning for Medical Image Computing*, 2020.

[32] C. You, N. Chen, and Y. Zou, "Contextualized attention-based knowledge transfer for spoken conversational question answering," in *INTERSPEECH*, 2021.

[33] C. You, N. Chen, F. Liu, D. Yang, and Y. Zou, "Towards data distillation for end-to-end spoken conversational question answering," *arXiv preprint arXiv:2010.08923*, 2020.

[34] L. Yang, R. P. Ghosh, J. M. Franklin, S. Chen, C. You, R. R. Narayan, M. L. Melcher, and J. T. Liphardt, "Nuset: A deep learning tool for reliably separating and analyzing crowded cells," *PLoS computational biology*, 2020.

[35] N. Chen, F. Liu, C. You, P. Zhou, and Y. Zou, "Adaptive bi-directional attention: Exploring multi-granularity representations for machine reading comprehension," in *ICASSP*, 2020.

[36] N. Chen, C. You, and Y. Zou, "Self-supervised dialogue learning for spoken conversational question answering," in *INTERSPEECH*, 2021.

[37] C. You, N. Chen, and Y. Zou, "Knowledge distillation for improved accuracy in spoken question answering," in *ICASSP*, 2021.

[38] C. You, Y. Zhou, R. Zhao, L. Staib, and J. S. Duncan, "Simcvd: Simple contrastive voxel-wise representation distillation for semi-supervised medical image segmentation," *arXiv preprint arXiv:2108.06227*, 2021.

[39] C. You, N. Chen, and Y. Zou, "MRD-Net: Multi-Modal Residual Knowledge Distillation for Spoken Question Answering," in *IJCAI*, 2021.

[40] ——, "Self-supervised contrastive cross-modality representation learning for spoken question answering," in *Findings of the Association for Computational Linguistics: EMNLP*, 2021.

[41] C. You, L. Han, A. Feng, R. Zhao, H. Tang, and W. Fan, "Megan: Memory enhanced graph attention network for space-time video super-resolution," in *WACV*, 2022.

[42] W. Xu, P. Zhou, C. You, and Y. Zou, "Semantic transportation prototypical network for few-shot intent detection," in *INTERSPEECH*, 2021.

[43] F. Liu, X. Wu, C. You, S. Ge, Y. Zou, and X. Sun, "Aligning source visual and target language domains for unpaired video captioning," *IEEE Transactions on Pattern Analysis and Machine Intelligence*, 2021.

[44] F. Liu, C. You, X. Wu, S. Ge, X. Sun *et al.*, "Auto-encoding knowledge graph for unsupervised medical report generation," in *NeurIPS*, 2021.

[45] C. You, R. Zhao, F. Liu, S. Chinchali, U. Topcu, L. Staib, and J. S. Duncan, "Class-aware generative adversarial transformers for medical image segmentation," *arXiv preprint arXiv:2201.10737*, 2022.

[46] B. Abdulhai, R. Pringle, and G. J. Karakoulas, "Reinforcement learning for true adaptive traffic signal control," *Journal of Transportation Engineering*, vol. 129, no. 3, pp. 278–285, 2003.

[47] L. Prashanth and S. Bhatnagar, "Reinforcement learning with function approximation for traffic signal control," *IEEE Transactions on Intelligent Transportation Systems*, vol. 12, no. 2, pp. 412–421, 2010.

[48] H. Wei, N. Xu, H. Zhang, G. Zheng, X. Zang, C. Chen, W. Zhang, Y. Zhu, K. Xu, and Z. Li, "Colight: Learning network-level cooperation for traffic signal control," in *Proceedings of the 28th ACM International Conference on Information and Knowledge Management*, 2019, pp. 1913–1922.

[49] G. Zheng, Y. Xiong, X. Zang, J. Feng, H. Wei, H. Zhang, Y. Li, K. Xu, and Z. Li, "Learning phase competition for traffic signal control," in *Proceedings of the 28th ACM International Conference on Information and Knowledge Management*, 2019, pp. 1963–1972.

[50] C. Chen, H. Wei, N. Xu, G. Zheng, M. Yang, Y. Xiong, K. Xu, and Z. Li, "Toward a thousand lights: Decentralized deep reinforcement learning for large-scale traffic signal control," *Proceedings of the AAAI Conference on Artificial Intelligence*, vol. 34, no. 04, pp. 3414–3421, Apr. 2020. [Online]. Available: https://ojs.aaai.org/index.php/AAAI/article/view/5744

[51] X. Zang, H. Yao, G. Zheng, N. Xu, K. Xu, and Z. Li, "Metalight: Value-based meta-reinforcement learning for traffic signal control," *Proceedings of the AAAI Conference on Artificial Intelligence*, vol. 34, no. 01, pp. 1153–1160, Apr. 2020.

[52] S. El-Tantawy, B. Abdulhai, and H. Abdelgawad, "Multiagent reinforcement learning for integrated network of adaptive traffic signal controllers (marlin-atsc): methodology and large-scale application on downtown toronto," *IEEE Transactions on Intelligent Transportation Systems*, vol. 14, no. 3, pp. 1140–1150, 2013.

[53] M. Aslani, M. S. Mesgari, and M. Wiering, "Adaptive traffic signal control with actor-critic methods in a real-world traffic network with different traffic disruption events," *Transportation Research Part C: Emerging Technologies*, vol. 85, pp. 732–752, 2017.

[54] B. Xu, Y. Wang, Z. Wang, H. Jia, and Z. Lu, "Hierarchically and cooperatively learning traffic signal control," in *Proceedings of the AAAI Conference on Artificial Intelligence*, vol. 35, 2021, pp. 669–677.

[55] H. Wei, G. Zheng, V. Gayah, and Z. Li, "A survey on traffic signal control methods," *arXiv preprint arXiv:1904.08117*, 2019.

[56] J. Gajda, R. Sroka, M. Stencel, A. Wajda, and T. Zeglen, "A vehicle classification based on inductive loop detectors," in *IMTC 2001. Proceedings of the 18th IEEE Instrumentation and Measurement Technology Conference. Rediscovering Measurement in the Age of Informatics*, vol. 1. IEEE, 2001, pp. 460–464.

[57] A. Buchenscheit, F. Schaub, F. Kargl, and M. Weber, "A vanet-based emergency vehicle warning system," in *2009 IEEE Vehicular Networking Conference (VNC)*. IEEE, 2009, pp. 1–8.

[58] Y. Wang, Z. Wu, X. Yang, and L. Huang, "Design and implementation of an emergency vehicle signal preemption system based on cooperative vehicle-infrastructure technology," *Advances in Mechanical Engineering*, vol. 5, p. 834976, 2013.

[59] H. Noori, L. Fu, and S. Shiravi, "A connected vehicle based traffic signal control strategy for emergency vehicle preemption," in *Transportation Research Board 95th Annual Meeting, Report Np. 16-6763*, 2016.

[60] H. Su, Z. Ji, K. Johansson, L. Jin *et al.*, "A hybrid queuing model for coordinated vehicle platooning on mixed-autonomy highways: Training and validation," *arXiv preprint arXiv:2103.14202*, 2021.

[61] J. Foerster, N. Nardelli, G. Farquhar, T. Afouras, P. H. Torr, P. Kohli, and S. Whiteson, "Stabilising experience replay for deep multi-agent reinforcement learning," in *International conference on machine learning*. PMLR, 2017, pp. 1146–1155.

[62] H. Su, K. Shi, J. Y. J. Chow, and L. Jin, "Dynamic queue-jump lane for emergency vehicles under partially connected settings: A multi-agent deep reinforcement learning approach," 2021.

Supplementary Material

S1 Related Work:

Conventional routing optimization and traffic signal pre-emption for EMVs. Although, in reality, routing and pre-emption are coupled, the existing methods usually solve them separately. Many of the existing approaches leverage Dijkstra's shortest path algorithm to get the optimal route [11–14]. An A* algorithm for ambulance routing has been proposed by [15]. However, as this line of work assumes that the routes and traffic conditions are fixed and static, they fail to address the dynamic nature of real-world traffic flows. Another line of work has considered the change of traffic flows over time. [16] has proposed a shortest-path algorithm for time-dependent traffic networks, but the travel time associated with each edge at each time step is assumed to be known in prior. [17] proposes different routing strategies for different times in a day (e.g., peak/non-peak hours) based on traffic history data at those times. However, in the problem of our consideration, routing and pre-emption strategies can significantly affect the travel time associated with each edge during the EMV passage, and the existing methods cannot deal with this kind of real-time changes. [18] formulated the dynamic shortest path problem as a mixed-integer programming problem. [19] has used RL for real-time vehicle navigation and routing. However, both of these studies have tackled a general routing problem, and signal pre-emption and its influence on traffic have not been modeled. Once an optimal route for the EMV has been determined, traffic signal pre-emption is deployed. A common pre-emption strategy is to extend the green phases of green lights to let the EMV pass each intersection along a fixed optimal route [11, 6]. [20] has proposed pre-emption strategies for multiple EMV requests. Please refer to [21] and [22] for a thorough survey of conventional routing optimization and traffic signal pre-emption methods. We would also like to point out that the conventional methods prioritize EMV passage and have significant disturbances on the traffic flow which increases the average non-EMV travel time.

RL-based traffic signal control. Traffic signal pre-emption only alters the traffic phases at the intersections where an EMV travels through. However, to reduce congestion, traffic phases at nearby intersections also need to be changed cooperatively. Recently, deep neural network has the promise to revolutionize the real world applications, especially in the context of healthcare and humanitarian assistance [23–45]. The coordination of traffic signals to mitigate traffic congestion is referred to as traffic signal control which has been addressed by leveraging deep RL in a growing body of work. Many of the existing approaches use Q-learning [46, 47, 3, 48–50]. [51] leverages meta-learning algorithms to speed up Q-learning for traffic signal control. Another line of work has used actor-critic algorithms for traffic signal control [52, 53, 4]. [54] proposes a hierarchical actor-critic method to encourage cooperation between intersections. Please refer to [55] for a review on traffic signal control methods. However, these RL-based traffic control methods focus on reducing the congestion in the traffic network and are not designed for EMV pre-emption. In contrast, our RL framework is built upon state-of-the-art ideas such as max pressure and is designed to reduce both EMV travel time and overall congestion.

S2 Justification of the Agent Design

The quantities in local agent state can be obtained at each intersection using various technologies. Numbers of vehicles on each lane $(x^t(l), x^t(m))$ can be obtained by vehicle detection technologies, such as inductive loop [56] based on the hardware installed underground. The distance of the EMV to the intersection $d^t_{EMV}[L_{ji}]$ can be obtained by *vehicle-to-infrastructure* technologies such as VANET [57], which broadcasts the real-time position of a vehicle to an intersection. Prior work [58–60] has explored these technologies for traffic signal pre-emption.

The dynamic routing algorithm (Algorithm 1) can provide $(\mathsf{ETA}, \mathsf{Next})$ for each agent at every time step. However, due to the stochastic nature of traffic flows, updating the route too frequently might confuse the EMV driver, since the driver might be instructed a new route, say, every 5 seconds. There are many ways to ensure reasonable frequency. One option is to inform the driver only once while the EMV is travels in a single link. We implement it by updating the state of an RL agent $(\mathsf{ETA}_i^{t'}, \mathsf{Next}_i^{t'})$ at the time step when the EMV travels through half of a link. For example, if the EMV travels through a link to agent i from time step 11 to 20 in constant speed, then dynamic routing information in s_i^{16} to s_i^{20} are the same, which is $(\mathsf{ETA}_i^{15}, \mathsf{Next}_i^{15})$, i.e., $t' = 15$.

As for the reward design, one might wonder how an agent can know its type. As we assume an agent can observe the state of its neighbors, agent type can be inferred from the observation. This will become clearer below.

S3 Multi-agent Actor Critic Method

Local Observation. In an ideal setting, agents can observe the states of every other agent and leverage this global information to make a decision. However, this is not practical in our problem due to communication latency and will cause scalability issues. We assume agents can observe its own state and the states of its neighbors, i.e., $s_{\mathcal{V}_i}^t = \{s_j^t | j \in \mathcal{V}_i\}$. The agents feed this observation to its policy network π_{θ_i} and value network V_{ϕ_i}.

Fingerprint. In multi-agent training, each agent treats other agents as part of the environment, but the policy of other agents are changing over time. [61] introduces *fingerprints* to inform agents about the changing policies of neighboring agents in multi-agent Q-learning. [4] brings fingerprints into MA2C. Here we use the probability simplex of neighboring policies $\pi_{\mathcal{N}_i}^{t-1} = \{\pi_j^{t-1} | j \in \mathcal{N}_i\}$ as fingerprints, and include it into the input of policy network and value network. Thus, our policy network can be written as $\pi_{\theta_i}(a_i^t | s_{\mathcal{V}_i}^t, \pi_{\mathcal{N}_i}^{t-1})$ and value network as $V_{\phi_i}(\tilde{s}_{\mathcal{V}_i}^t, \pi_{\mathcal{N}_i}^{t-1})$, where $\tilde{s}_{\mathcal{V}_i}^t$ is the local observation with spatial discount factor, which is introduced below.

Spatial Discount Factor and Adjusted Reward. MA2C agents cooperatively optimize a global cumulative reward. We assume the global reward is decomposable as $r_t = \sum_{i \in \mathcal{V}} r_i^t$, where r_i^t is defined in Eqn. 1. Instead of optimizing the same global reward for every agent, [4] proposes a spatial discount factor α to let each agent pay less attention to rewards of agents far away. The adjusted reward for agent i is

$$\tilde{r}_i^t = \sum_{d=0}^{D_i} \Big(\sum_{j \in \mathcal{V} | d(i,j)=d} (\alpha)^d r_j^t \Big), \tag{2}$$

where D_i is the maximum distance of agents in the graph from agent i. When $\alpha > 0$, the adjusted reward include global information, it seems this is in contradiction to the local communication assumption. However, since reward is only used for offline training, global reward information is allowed. Once trained, the RL agents can control traffic signal without relying on global information.

Temporal Discount Factor and Return. The local return $\tilde{R}_i^t$ is defined as the cumulative adjusted reward $\tilde{R}_i^t := \sum_{\tau=t}^{T} \gamma^{\tau - t} \tilde{r}_i^\tau$, where γ is the temporal discount factor and T is the length of an episode. we can estimate the local return using value function,

$$\tilde{R}_i^t = \tilde{r}_i^t + \gamma V_{\phi_i^-}(\tilde{s}_{\mathcal{V}_i}^{t+1}, \pi_{\mathcal{N}_i}^t | \pi_{\theta_{-i}^-}), \tag{3}$$

where ϕ_i^- means parameters ϕ_i are frozen and θ_{-i}^- means the parameters of policy networks of all other agents are frozen.

Network architecture and training. As traffic flow data are spatial temporal, we leverage a long-short term memory (LSTM) layer along with fully connected (FC) layers for policy network (actor) and value network (critic). Our multi-agent actor-critic training pipeline is similar to that in [4]. We provide neural architecture details, policy loss expression, value loss expression as well as a training pseudocode.

S4 Training Details

S4.1 Value loss function

With a batch of data $B = \{(s_i^t, \pi_i^t, a_i^t, s_i^{t+1}, r_i^t)_{i \in \mathcal{V}}^{t \in \mathcal{T}}\}$, each agent's value network is trained by minimizing the difference between bootstrapped estimated value and neural network approximated value

$$\mathcal{L}_v(\phi_i) = \frac{1}{2|B|} \sum_B \Big(\tilde{R}_i^t - V_{\phi_i}(\tilde{s}_{\mathcal{V}_i}^t, \pi_{\mathcal{N}_i}^{t-1}) \Big)^2. \tag{4}$$

S4.2 Policy loss function

Each agent's policy network is trained by minimizing its policy loss

$$\mathcal{L}_p(\theta_i) = -\frac{1}{|B|}\sum_{B}\Bigg(\log \pi_{\theta_i}(a_i^t|s_{\mathcal{V}_i}^t, \pi_{\mathcal{N}_i}^{t-1})\tilde{A}_i^t \tag{5}$$

$$- \lambda \sum_{a_i \in \mathcal{A}_i} \pi_{\theta_i} \log \pi_{\theta_i}(a_i|s_{\mathcal{V}_i}^t, \pi_{\mathcal{N}_i}^{t-1})\Bigg), \tag{6}$$

where $\tilde{A}_i^t = \tilde{R}_i^t - V_{\phi_i^-}(\tilde{s}_{\mathcal{V}_i}^t, \pi_{\mathcal{N}_i}^{t-1})$ is the estimated advantage which measures how much better the action a_i^t is as compared to the average performance of the policy π_{θ_i} in the state s_i^t. The second term is a regularization term that encourage initial exploration, where $\mathcal{A}_i$ is the action set of agent i. For an intersection as shown in Fig. 1, $\mathcal{A}_i$ contains 8 traffic signal phases.

S4.3 Training algorithm

Algorithm S1 shows the multi-agent A2C training process.

Algorithm S1: Multi-agent A2C Training

Input :

T	maximum time step of an episode
N_{bs}	batch size
η_θ	learning rate for policy networks
η_ϕ	learning rate for value networks
α	spatial discount factor
γ	(temporal) discount factor
λ	regularizer coefficient

Output :

$\{\phi_i\}_{i\in\mathcal{V}}$	learned parameters in value networks
$\{\theta_i\}_{i\in\mathcal{V}}$	learned parameters in policy networks

initialize $\{\phi_i\}_{i\in\mathcal{V}}$, $\{\theta_i\}_{i\in\mathcal{V}}$, $k \leftarrow 0$, $B \leftarrow \varnothing$; **initialize** SUMO, $t \leftarrow 0$, **get** $\{s_i^0\}_{i\in\mathcal{V}}$
repeat
  `/* generate trajectories */`
  foreach $i \in \mathcal{V}$ **do (in parallel)**
    sample a_i^t from π_i^t
    receive $\tilde{r}_i^t$ and s_i^{t+1}
  $B \leftarrow B \cup \{(s_i^t, \pi_i^t, a_i^t, s_i^{t+1}, r_i^t)_{i\in\mathcal{V}}\}$
  $t \leftarrow t+1, k \leftarrow k+1$
  if $t == T$ **then**
    initialize SUMO, $t \leftarrow 0$, **get** $\{s_i^0\}_{i\in\mathcal{V}}$
  `/* update actors and critics */`
  if $k == N_{\text{bs}}$ **then**
    foreach $i \in \mathcal{V}$ **do (in parallel)**
      calculate $\tilde{r}_i^t$ (Eqn. (4)), $\tilde{R}_i^t$ (Eqn. (5))
      $\phi_i \leftarrow \phi_i - \eta_\phi \nabla \mathcal{L}_v(\phi_i)$
      $\theta_i \leftarrow \theta_i - \eta_\theta \nabla \mathcal{L}_p(\theta_i)$
    $k \leftarrow 0, B \leftarrow \varnothing$
until *Convergence*

S5 Intralink EMV travel time

The intra-link traffic pattern with the presence of an EMV on duty is complicated and is under-explored in the current literature. For simplicity, here we demonstrate a simple intra-link traffic model for a link with 2 lanes. The model can be easily extended for multiple lanes.

In a two-lane link, the EMV takes a lane and the non-EMVs on the other lane usually slows down or entirely stop. Some non-EMVs ahead of the EMV find pull-over spots in the other lane and park there. Those that cannot find a parking spot continue to drive in front of the EMV, potentially blocking

the EMV passage [62]. In this study, we propose a meso-scopic model to estimate the intra-link travel time of an EMV. Normally, the traffic flow of a link is modeled by a fundamental diagram, see

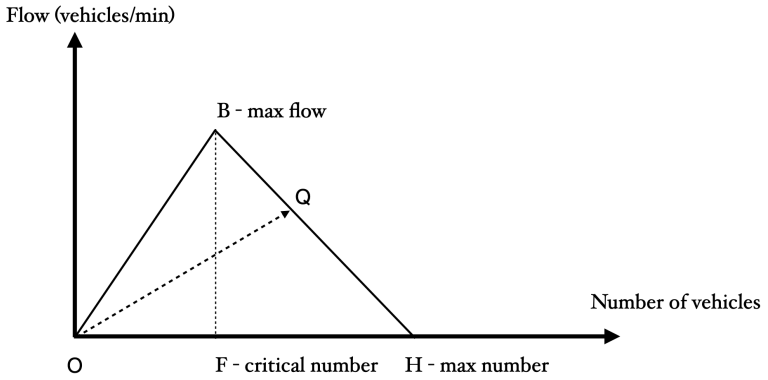


Figure 5: Normal traffic state.

Fig 5. This diagram depicts a simplified relationship between the flow rate, i.e. number of vehicles passing within the unit amount of the time, and number of vehicles on a link. The max number of vehicles H indicates the capacity of this link. The critical number of vehicles F indicates the boundary differentiates the non-congested state and congested state. When the number of vehicles is smaller than F, all vehicles are traveling at the free flow speed, which is represented by the slope of OB. When number of vehicles is larger than F, vehicles are slowing down and traffic flows declines since the link is now congested. The max flow is attained when the number of vehicles is at F. The travel speed of vehicles in a congested state Q is obtained by the slope of OQ.

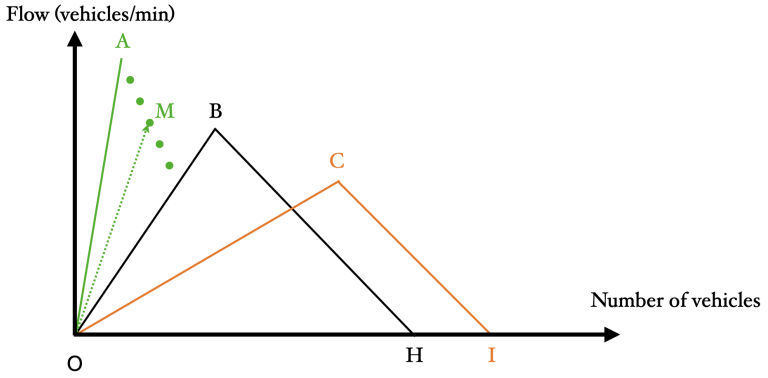


Figure 6: Traffic state during EMV pre-emption.

During the EMV pre-emption, the original traffic flow relationship pictured in black are diverted into two parts, representing two lanes respectively. The green line represents the traffic conditions of the pre-emption lane, i.e. the lane where the EMV is traveling, and the orange line represents the other lane. During pre-emption, part of the vehicles originally travelling in front of the EMV pull over onto the adjacent lane, resulting a significant decrease in the max capacities of the pre-emption lane. Meanwhile, because vehicles can park onto the curbs, orange line depicts a larger maximum capacity I than normal.

Regarding the max flow, the adjacent lane has a smaller max flow as the vehicles on this lane are required to slow down when EMV is on duty. The pre-emption lane obtains a max capacity when there is one vehicle on the lane, i.e. the EMV itself. Under this circumstance, the flow rate is

equivalent as the free flow speed of the EMV. However, when there are vehicles remaining in front of the EMV, the travel speed of the EMV might be slowed down, but still higher than the free flow speeds of the non-EMVs. Furthermore, the travel speed of EMV has a discrete value corresponding to the number of non-EMVs blocking. For example, pre-emption lane has a traffic state represented by M, and the travel speed of the EMV is obtained as the slope of M. We use this simple model, especially the green plot to estimate the intra-link travel time of EMV in a link as a function of number of vehicles in that link. We calibrate this model with the SUMO environment. Intuitively, the travel speed of the EMV is affected more by the number of vehicles on the pre-emption lane than their positions. The reason behind is since the ETA is frequently updated every ΔT seconds (ΔT in our experiment), and the estimated ETA would eventually converge. Imagine there are vehicles very far away from the EMV and about to leave the intersections at t, their presence would not slow down the approaching EMV. Therefore, when they have left the intersection at $t+1$, we have an updated number of non-EMVs count and updated travel speed estimation.

S6 Implementation Details

Although MDP step length can be arbitrarily small enough for optimality, traffic signal phases should maintained a minimum amount of time so that vehicles and pedestrians can safely cross the intersections. To avoid rapid switching between the phases, we set our MDP time step length to be 5 seconds.

S6.1 Implementation details for synthetic grid$_{5\times5}$

- dimension of $s^t_{\mathcal{V}_i}$: $5 \times (8+8+4+2) = 110$
- dimension of $\tilde{s}^t_{\mathcal{V}_i}$: $5 \times (8+8+4+2) = 110$
- dimension of $\pi^{t-1}_{\mathcal{N}_i}$: $4 \times 8 = 32$
- Policy network $\pi_{\theta_i}(a^t_i | s^t_{\mathcal{V}_i}, \pi^{t-1}_{\mathcal{N}_i})$: `concat[`110 $\xrightarrow{\text{FC}}$ 128ReLu, 32 $\xrightarrow{\text{FC}}$ 64ReLu`]` $\rightarrow$ 64LSTM $\xrightarrow{\text{FC}}$ 8Softmax
- Value network $V_{\phi_i}(\tilde{s}^t_{\mathcal{V}_i}, \pi^{t-1}_{\mathcal{N}_i})$: `concat[`110 $\xrightarrow{\text{FC}}$ 128ReLu, 32 $\xrightarrow{\text{FC}}$ 64ReLu`]` $\rightarrow$ 64LSTM $\xrightarrow{\text{FC}}$ 1Linear
- Each link is $200m$. The free flow speed of the EMV is $12m/s$ and the free flow speed for non-EMVs is $6m/s$.
- Temporal discount factor γ is 0.99 and spatial discount factor α is 0.90.
- Initial learning rates η_ϕ and η_θ are both 1e-3 and they decay linearly. Adam optimizer is used.
- MDP step length $\Delta t = 5s$ and for secondary pre-emption reward weight β is 0.5.
- Regularization coefficient is 0.01.

S6.2 Implementation details for Manhattan$_{16\times3}$

The implementation is similar to the synthetic network implementation, with the following differences:

- Initial learning rates η_ϕ and η_θ are both 5e-4.
- Since the avenues and streets are both one-directional, the number of actions of each agent are adjusted accordingly.

S7 Ablation Study

S7.1 Ablation study on pressure and agent types

We propose three types of agents and design their rewards (Eqn. 1) based on our improved pressure definition and heuristics. In order to see how our improved pressure definition and proposed special agents influence the results, we (1) replace our pressure definition by that defined in PressLight, (2) replace secondary pre-emption agents with normal agents and (3) replace primary pre-emption agents with normal agents.

Ablations	(1)	(2)	(3)	EMVLight
T_{EMV} [s]	**197**	289	320	199
T_{avg} [s]	361.05	347.13	359.62	**322.40**

Table 2: Ablation study on pressure and agent types. Experiments are conducted on the Config 1 synthetic grid$_{5\times5}$.

Table 2 shows the results of these ablations: (1) PressLight-style pressure (see Appendix) yields a slightly smaller EMV travel time but significantly increases the average travel time; (2) Without secondary pre-emption agents, EMV travel time increases by 45% since almost no “link reservation" happened; (3) Without primary pre-emption agents, EMV travel time increases significantly, which shows the importance of pre-emption.

S7.2 Ablation study on fingerprint

In multi-agent RL, fingerprint has been shown to stabilize training and enable faster convergence. In order to see how fingerprint affects training in EMVLight, we remove the fingerprint design, i.e., policy and value networks are changed from $\pi_{\theta_i}(a_i^t|s_{\mathcal{V}_i}^t, \pi_{\mathcal{N}_i}^{t-1})$ and $V_{\phi_i}(\tilde{s}_{\mathcal{V}_i}^t, \pi_{\mathcal{N}_i}^{t-1})$ to $\pi_{\theta_i}(a_i^t|s_{\mathcal{V}_i}^t)$ and $V_{\phi_i}(\tilde{s}_{\mathcal{V}_i}^t)$, respectively. Fig. 7 shows the influence of fingerprint on training. With fingerprint, the reward converges faster and suffers from less fluctuation, confirming the effectiveness of fingerprint.

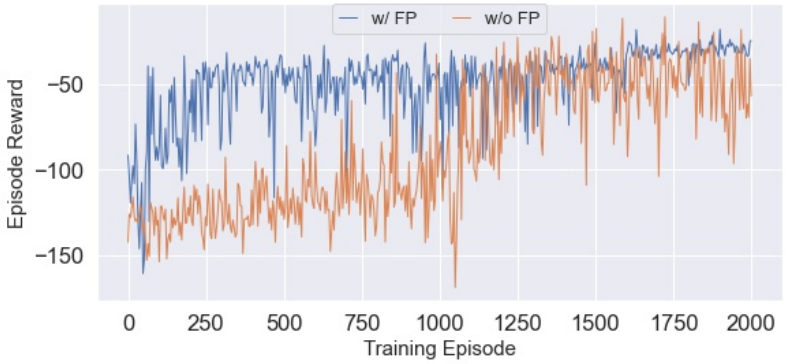


Figure 7: Reward convergence with and without fingerprint. Experiments are conducted on Config 1 synthetic grid$_{5\times5}$.